Journal of
Applied Crystallography
ISSN 0021-8898
Editor: **Anke R. Kaysser-Pyzalla**

X-ray phase measurements as a probe of small structural changes in doped nonlinear optical crystals

Sérgio L. Morelhão, Claúdio M. R. Remédios, Raul O. Freitas and Adenilson O. dos Santos

J. Appl. Cryst. (2011). **44**, 93–101

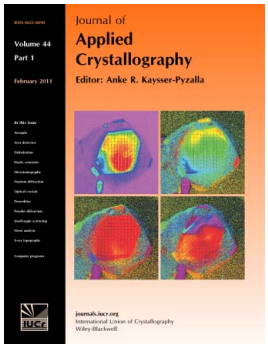

Journal of
Applied Crystallography
ISSN 0021-8898

Received 8 April 2010
Accepted 19 October 2010

X-ray phase measurements as a probe of small structural changes in doped nonlinear optical crystals

Sérgio L. Morelhão,[a]* Claúdio M. R. Remédios,[b] Raul O. Freitas[a] and Adenilson O. dos Santos[c]

[a]Instituto de Física, Universidade de São Paulo, CP 66318, 05315-970 São Paulo, SP, Brazil, [b]Faculdade de Física, Universidade Federal do Pará, Belém, PA, Brazil, and [c]CCSST, Universidade Federal do Maranhão, Imperatriz, MA, Brazil. Correspondence e-mail: morelhao@if.usp.br

X-ray multiple diffraction experiments with synchrotron radiation were carried out on pure and doped nonlinear optical crystals: $NH_4H_2PO_4$ and KH_2PO_4 doped with Ni and Mn, respectively. Variations in the intensity profiles were observed from pure to doped samples, and these variations correlated with shifts in the structure factor phases, also known as triplet phases. This result demonstrates the potential of X-ray phase measurements to study doping in this type of single crystal. Different methodologies for probing structural changes were developed. Dynamical diffraction simulations and curve fitting procedures were also necessary for accurate phase determination. Structural changes causing the observed phase shifts are discussed.

1. Introduction

The physical properties of materials are in general intrinsically related to their crystal structures. Many materials with very interesting physical properties for technological applications can be grown or synthesized as single crystals, *e.g.* semiconductors, ferroelectrics, multiferroics, piezoelectrics and others. Single-crystal forms of materials are necessary in certain applications, as in the case of nonlinear optical (NLO) crystals, widely used in laser technology. Controlling materials properties is one of the most fundamental goals in the science and engineering of materials. In terms of current trends in designing technological crystals, quantifying correlations between variations of physical properties and very small changes of crystal structure can be the key to acquiring knowledge of the physics involved and to allow the efficient design of new materials with improved properties. Methods for monitoring small structural changes are therefore important. Although there are well established methods for probing crystal structures, mostly X-ray diffraction methods, the scope of conditions in which these methods can be applied is limited. This is where alternative methods suitable for unusual conditions can be helpful in studying technological crystals.

Since it was reported decades ago that information on the phases of the structure factors – or more precisely, on invariant triplet phases – could be accessed *via* X-ray multiple diffraction (XRMD) experiments (Lipscomb, 1949; Hart & Lang, 1961; Post, 1977; Chapman *et al.*, 1981; Chang, 1984; Shen & Colella, 1987), many attempts have been made to use this phenomenon as a physical solution of the phase problem in X-ray crystallography or, at least, as a general tool for studying crystalline and nonperiodic materials (Tischler & Batterman, 1986; Rossmanith, 1992; Weckert & Hümmer, 1997; Avanci *et al.*, 1998; Stetsko *et al.*, 2000, 2001; Shen *et al.*, 2000; Remédios *et al.*, 2005). In this latter context, XRMD can be seen as a method to provide specific pieces of information that could not be retrieved by any other method and thus make it possible to distinguish one atomic structure from another among several possibilities. For instance, this was demonstrated in elucidating the mechanism of resonant scattering in $LaMnO_3$ (Shen *et al.*, 2006). However, the potential field of applications of XRMD in phase measurements is not widely exploited. It has potential for new opportunities in the dynamical theory of X-ray diffraction beyond of the usual two-beam diffraction cases. Phase sensitivity in XRMD experiments is due to interference of simultaneously diffracted waves inside the crystal, which is essentially a dynamical diffraction process that can be described by the *N*-beam dynamical theory in perfect crystal slabs (Colella, 1974; Chang, 1984; Weckert & Hümmer, 1997). There is, however, a difficult point to be settled, which is how to account for crystalline imperfections and their influence on the dynamical interference of the X-ray waves undergoing multiple diffraction.

In this work, we experimentally exploited the potential of XRMD phase measurements for investigating small changes of fractional coordinates (of the atoms in the unit cell), such as those caused by internal stresses (Reeuwijk *et al.*, 2000) in doped NLO crystals. In particular, we studied ADP (ammonium dihydrogen phosphate, $NH_4H_2PO_4$) and KDP (potassium dihydrogen phosphate, KH_2PO_4) doped with Ni and Mn, respectively. In the former, remarkable phase shifts were obtained, which could be correlated to an increased disorder of oxygen sites due to doping. For the sake of comparison,

similar phase shifts were induced in a GaAs crystal by changing the X-ray energy. In the case of Mn-doped KDP, the polarization and energy of the synchrotron radiation were adjusted to enhance the phase sensitivity for quantitative data analysis. Samples with different contents of Mn in the crystal lattice were investigated. The influence of lattice imperfections on measured phase values was minimized by using a criterion to identify XRMD cases suitable for accurate phasing. Structural changes in the doped samples accounting for the observed phase shifts are discussed.

2. Theoretical aspects

Phases of single reflections, *i.e.* structure factor phases, are values relative to the choice of origin. For instance, $F'(\mathbf{Q}) = \exp(i\mathbf{Q}\cdot\Delta\mathbf{r})F(\mathbf{Q})$ would be the structure factor for an arbitrary choice that is displaced $\Delta\mathbf{r}$ from the origin used to calculate $F(\mathbf{Q})$ for the diffraction vector $\mathbf{Q}$. The same dependence of origin choice does not occur for structure factor triplets such as

$$\frac{F'(\mathbf{B})F'(\mathbf{C})}{F'(\mathbf{A})} = \frac{|F(\mathbf{B})||F(\mathbf{C})|}{|F(\mathbf{A})|}\exp\{i[\Psi + (\mathbf{B}+\mathbf{C}-\mathbf{A})\cdot\Delta\mathbf{r}]\}, \quad (1)$$

where $\Psi = \delta_B + \delta_C - \delta_A$, δ_Q is the phase of the structure factor $F(\mathbf{Q})$ and the diffraction vectors fulfill the relationship $\mathbf{B}+\mathbf{C}-\mathbf{A}=0$. The phase triplet, or triplet phase, Ψ is therefore invariant regarding the choice of origin, and it is a physically measurable quantity *via* XRMD experiments (Hart & Lang, 1961; Post, 1977; Chapman *et al.*, 1981; Chang, 1984; Weckert & Hümmer, 1997).

For a short overview of the XRMD method, consider the structure factor triplet already given in equation (1) for the Bragg reflections A, B and C. The XRMD profile obtained by measuring reflection A, while tuning and detuning reflection B, is sensitive to the triplet phase Ψ. It also corresponds to the phase difference between the primary wave, from primary reflection A, and the secondary wave that is systematically generated when reflection B is tuned. This secondary wave has been scattered twice: first on reflection B, and then on reflection C, as detailed elsewhere (Giacovazzo, 2002; Morelhão & Kycia, 2002; dos Santos *et al.*, 2009). Henceforth, we will refer to each XRMD case by the indices of the reflections $B\&C$ whose sum provides the indices of reflection A, *i.e.* $h_A = h_B + h_C$, $k_A = k_B + k_C$ and $\ell_A = \ell_B + \ell_C$, or, occasionally, only by the indices of reflection B.

As a function of the triplet phases, the XRMD profiles typically have an asymmetric character for Ψ values around 0 or 180°, and a symmetric character for values equal to ±90°. Fig. 1 shows examples of such behavior in a GaAs (002) crystal. At the X-ray energy $E = 10\,200$ eV, below the absorption edge of Ga (Figs. 1*a* and 1*c*), both XRMD cases have Ψ close to ±90°. Their profiles are nearly symmetric with a slight destructive/constructive type of asymmetry. Above the absorption edge (Figs. 1*b* and 1*d*), the triplet phases change by about 50° and the levels of asymmetry increase significantly in both profiles. Inversion of asymmetry, from destructive/constructive to constructive/destructive, is observed in one case (Fig. 1*d*), since the triplet phase of this case has moved from the first to the second quadrant, crossing the value of 90°.

An accurate description of the interference process is given by the N-beam dynamical theory of X-ray diffraction in perfect crystal slabs (Colella, 1974; Chang, 1984; Weckert & Hümmer, 1997). This allows simulation of the intrinsic dynamical profiles $I_{\rm dyn}(\omega,\varphi)$, as a function of the incidence ω and azimuthal φ angles. For triplet phase analysis *via* XRMD, the interference profiles are usually monitored by azimuthal scans of reflection A (φ scans; Renninger, 1937), as in Fig. 1, where the incidence angle ω is kept constant at ω_A, the central angle of reflection A whose value is equal to the Bragg angle plus a small correction to account for refraction. Instrumental parameters such as divergence, spectral bandwidth and mosaicity are taken into account by convolution of the intrinsic dynamical profile with a broadening function, in general a suitable Gaussian G with standard deviations σ_ω and σ_φ with regard to the ω and φ axes of rotation, respectively (Weckert & Hümmer, 1997). Then, $I(\varphi) = [I_{\rm dyn} * G]$ $(\omega = \omega_A, \varphi)$ is the simulated profile to be compared with the experimental ones.

Inevitably, measurements of triplet phases *via* XRMD always raise questions of how good, from a crystallographic viewpoint, the sample has to be for this method to work. This is a crucial point in studying doped NLO crystals. When comparing intensity profiles from pure and from doped samples, inversion of profile asymmetry is strong evidence of changes in the reflection phases. The presence of lattice defects, such as grain boundaries in mosaic crystals, can destroy the interference of the diffracted waves, leading to profiles that look more symmetric. However, inversion of

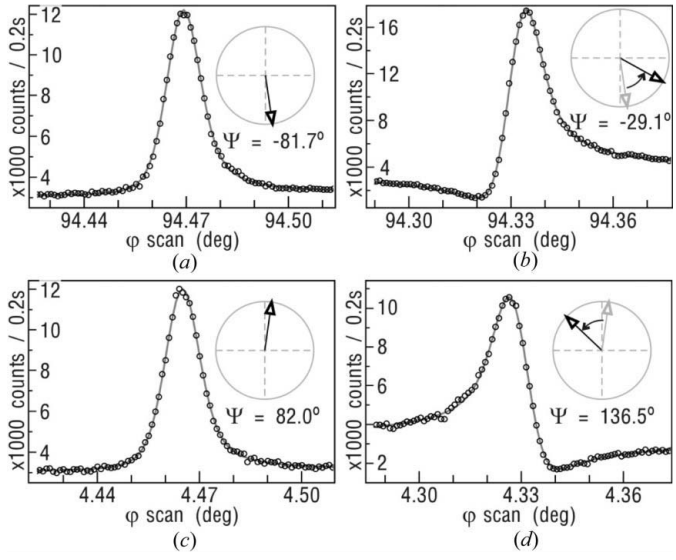

Figure 1
Experimental (open circles) XRMD interference profiles in a GaAs (002) crystal: (*a*), (*b*) 111&$\bar{1}\bar{1}1$, and (*c*), (*d*) $1\bar{1}1$&$\bar{1}11$ cases. X-ray energy: (*a*), (*c*) $E = 10\,200$ eV and (*b*), (*d*) $E = 10\,500$ eV. Reference direction: M = [$\bar{1}10$] (see *Experimental* section for details on data acquisition). Calculated triplet phases are shown beside each profile.

Table 1
Validity of X-ray multiple diffraction theories regarding crystal size and perfection.

$P(m)$ denotes the probability of photon–lattice interaction of mth order in single crystals (SC), as well as in one of many perfect diffracting regions (PDR) composing imperfect crystals (IC). Valid theoretical approaches are indicated by 'Yes', non-valid ones by 'No' and undefined situations by '?'. $P(m>1)\neq 0$ is required for accessing information on triplet phases.

		XRD theories		
Crystal size and perfection	Regime of diffraction	Kinematic	Dynamic	Second order [equation (2)]
Very small SC	$P(m>1)=0$	Yes	Yes	Yes ($\mathbf{D}_2=0$)
Small SC	$P(m>2)\simeq 0$	No	Yes	Yes ($\xi=1$)
Large SC	$P(m\geq 3)>>0$	No	Yes	?
IC with very small PDR	$P(m>1)=0$	Yes	No	Yes ($\xi=0$)
IC with small PDR	$P(m>2)\simeq 0$	No	?	Yes ($0<\xi<1$)
IC with large PDR	$P(m\geq 3)>>0$	No	?	?

asymmetry is an effect that does not seem possible by just increasing the mosaicity of the crystal. The problem of lattice imperfections is critical only when accurate measurements of phase shifts are desired. In this case, it is necessary to distinguish changes in the profile asymmetries caused by loss of crystalline quality from those caused by actual changes in the reflection phases.

An approach to identify XRMD cases that are highly susceptible to the presence of imperfections is possible. It is based on comparing the exact solution from N-beam dynamical theory and an approximated second-order series expansion solution of the diffraction process (Juretschke, 1982; Shen, 1998). Within the second-order approximation, the primary wave $\mathbf{D}_1$, from reflection A, and the secondary wave $\mathbf{D}_2$, from reflections B and C, lead to the expression

$$I_{2\mathrm{nd}}(\omega,\varphi)=|\mathbf{D}_1|^2+|\mathbf{D}_2|^2+\xi(\mathbf{D}_1\cdot\mathbf{D}_2^*+\mathbf{D}_1^*\cdot\mathbf{D}_2) \quad (2)$$

for the intrinsic profile. The interference term, which appears multiplied by ξ, is responsible for the information on triplet phases carried on by the XRMD profiles, and the parameter ξ has been introduced by hand in order to gauge the contribution of the interference term in the intensity profile (Morelhão, 2003*a*).

In the exact dynamical solution, all possible interactions of X-ray photons with the crystalline lattice are taken into account, which corresponds to a non-truncated series expansion solution. The number of interactions, however, depends on the size and perfection of the crystal (Thorkildsen *et al.*, 2003; Authier, 2005). A general overview of this dependence and the validity of the most common theoretical approaches (Chang, 1984; Rossmanith, 2007) are given in Table 1. In a small single crystal where the X-ray photons can interact at most twice, the XRMD process can be, in principle, described by equation (2) with $\xi=1$ (row 2 of Table 1). Equation (2) is also valid for large imperfect crystals where the perfect diffracting regions are small enough to eliminate the probability of a third intra-region interaction (row 5 of Table 1). However, in this case, $0<\xi<1$ since $|\mathbf{D}_2|^2$ also accounts for twice-diffracted photons among distinct regions without phase coherence (inter-region interaction, *i.e.* B and C reflections taking place at different perfect regions) (Morelhão, 2003*a*). Therefore, it is straightforward to conclude that XRMD profiles dominated by the second-order term, even in large single crystals, will not be severely affected by a reduction in the size of the perfect diffracting regions, since equation (2) is still valid. The problem is how to use this fact, in practice, to identify suitable XRMD cases for accurate triplet phase measurements.

The critical sizes of the single crystals (SC) or perfect diffracting regions (PDR) used in Table 1 can be specified with respect to the number N_e of diffracting planes fitted in the dynamical extinction distance of reflection B. In two-beam diffraction, a comparison of kinematical and dynamical calculations, such as the one performed by Authier (2005, equation 4.50), has shown that dynamical effects are negligible when the actual number N of diffracting planes is smaller than about one-tenth of N_e, *i.e.* $N/N_\mathrm{e}\leq 0.1$. This corresponds to the definition of very small SC or PDR in Table 1 (rows 1 and 4). Even under three-beam diffraction, this definition is valid since the diffracted waves are so weak that no coherent coupling is possible below this very small size limit. The definition of small SC or PDR (rows 2 and 5) falls in the size range where $0.1<N/N_\mathrm{e}<1$. The condition for X-ray photons to interact at most twice inside a small single crystal or perfect diffracting region also requires that $N/N_\mathrm{e}<1$ for both A and C reflections. Within the mosaic model of imperfect crystals, details about the perfect diffraction region size effects on XRMD intensity profiles can be found in the work by Thorkildsen *et al.* (2003).

Here, to analyze only the phase information in XRMD profiles, the line-profile function

$$L(\varphi)=[I_{2\mathrm{nd}}(\omega=\omega_A)*G](\varphi)/D_0^2 \quad (3)$$

will be used for curve fitting purposes. Equation (3) is derived from equation (2) when writing $\mathbf{D}_1=D_A\mathbf{v}_1[1-g|f(\varphi)|]^{1/2}$, $\mathbf{D}_2=RD_A\mathbf{v}_2 f(\varphi)\exp(i\Psi)$ and $D_0^2=|D_A\mathbf{v}_1|^2$ as the base-line intensity determined by the primary reflection A. Only the convolution with the Gaussian G regarding the φ axis is required. In the ω axis, the convolution is implied in the values of D_A, g, R and $f(\varphi)$. The D_A values disappear as a result of the normalization, and the others are adjustable parameters in the fitting process. $f(\varphi)=w_\mathrm{S}/[2(\varphi-\varphi_0)-iw_\mathrm{S}]$ imitates the dependence with the azimuthal φ angle, $w_\mathrm{S}=\pm w$ and w is the effective width of the azimuthal profiles (Morelhão & Kycia, 2002; Morelhão, 2003*a*). $g|f(\varphi)|$ is empirical and accounts for energy loss due to photons exiting the crystal through the diffracted beam from reflection B (the amount not coupled by reflection C) (Thorkildsen *et al.*, 2003; Morelhão *et al.*, 2005*a*). The polarization vectors $\mathbf{v}_{1,2}$ are computed for each polarization angle χ of the incident synchrotron radiation, as detailed in Appendix *A*. For each given value of Ψ, there are a total of six adjustable parameters in $L(\varphi)$, which are summarized in the parameter vector $\mathbf{p}=(w,R,\xi,g,\sigma_\varphi,\varphi_0)$. An evolutionary algorithm (Wormington *et al.*, 1999) has been used to adjust these parameters in $\mathbf{p}$ for a pre-fixed number of generations. The fitting evolution is driven by the least-mean

absolute deviation (LMAD) of $L(\varphi)$ with respect to a given azimuthal profile (simulated or experimental).

3. Experimental

NLO crystals were investigated at room temperature, in rectangular $a \times b \times c$ samples with dimensions greater than 5 mm along all axes. Pure and doped samples were grown from supersaturated aqueous solutions at pH 3.9 (1) at 313 K, an Ni-doped ADP sample (ADP:Ni) in a molar solution with 1% $NiCl_2{\cdot}6H_2O$ and 99% $NH_4H_2PO_4$, and Mn-doped KDP samples in 1% (KDP:Mn1) and 5% (KDP:Mn5) stoichiometric concentrations of $KMnO_4$ in a KH_2PO_4 solution. The actual amounts of Mn incorporated into the crystal lattice were verified by Rutherford backscattering (RBS) as being 0.001 and 0.009 mol of Mn per mol of KDP, or 0.04 and 0.36 wt% contents in the KDP:Mn1 and KDP:Mn5 samples, respectively.

XRMD experiments were carried out at diffraction station XRD1 of the Brazilian Synchrotron Light Laboratory (LNLS). Thus is a bending magnetic beamline with a focusing mirror, a two-bounce Si(111) monochromator with a sagittal second crystal and slit screens. The X-ray optics were in parallel beam mode (mirror and sagittal crystal focused at infinity): photon energy E with $\Delta E/E \simeq 2 \times 10^{-4}$, effective divergences of 18 (vertical) $\times$ 24 (horizontal) arcseconds, and incident beam size of 0.5 $\times$ 0.5 mm. The mechanical accuracy was 0.0002° in both ω and φ rotation axes.

In each sample, data acquisition was performed after aligning the diffraction vector **A** parallel to the φ rotation axis within a precision of about 0.002°. The angle of azimuth in which a chosen reference direction M is on the incidence plane of the diffractometer (pointing towards the X-ray source) corresponds to $\varphi = 0$. All φ scans were collected at the center of the rocking curve of reflection A, and they refer to a clockwise rotation of the reciprocal space, with vector **A** pointing towards the observer. The polarization angle χ allows the incidence plane to rotate around the incident beam direction: π and σ polarization for $\chi = 0°$ and $\chi = 90°$, respectively (Appendix A).

4. Results and discussions

4.1. ADP

Experimental φ scans in ADP and ADP:Ni samples are shown in Fig. 2. As can be noticed, the constructive/destructive pattern of interference is shifted along the scan of the doped sample. This fact suggests a phase shift of nearly 180° in the 400 reflection responsible for the base-line intensity. Similar to the 002 GaAs reflection of structure factor $F_{GaAs}(002) = 4(f_{As} - f_{Ga})$, the 400 ADP reflection is very weak since its structure factor is also proportional to a difference of atomic scattering factors, *i.e.* $F_{ADP}(400) \simeq 4(f_P + f_N - 2.754 f_O) = |F_A| \exp(i\delta_A)$. Consequently, the phase of this type of reflection can be shifted by several tens of degrees in response to a small change in the scattering properties of the atomic site.

In the case of Ni doping, a small increase in the disorder of the oxygen sites can induce such a large shift in δ_A, but this depends on the exact scattering amplitudes of the ions in the structure. For instance, the statistical distribution of misplaced oxygen is analogous to thermal vibration of the lattice and can be taken into account in a similar manner. Then, the structure factor of the 400 reflection in the ADP:Ni sample is written as

$$F_{ADP:Ni}(400) \simeq 4\{f_P + f_N - 2.754 f_O \exp[-8\pi^2 \langle \mathbf{u}^2 \rangle (\sin\theta/\lambda)^2] + \Delta\}, \quad (4)$$

where $\langle \mathbf{u}^2 \rangle$ is the mean-squared displacement of the O atoms owing to the presence of Ni^{2+} ions in the crystal lattice, $\Delta = (f_{P^{5+}} - f_P)_{Th} + (f_{NH_4^{1+}} - f_N)_{Th} - 2.754(f_{O^{2-}} - f_O)_{Th}$ denotes the overall difference in the actual Thomson scattering amplitudes regarding the tabulated values for neutral atoms, and θ and λ denote the Bragg angle and wavelength, respectively. Fig. 3 shows the phase angle of the 400 reflection

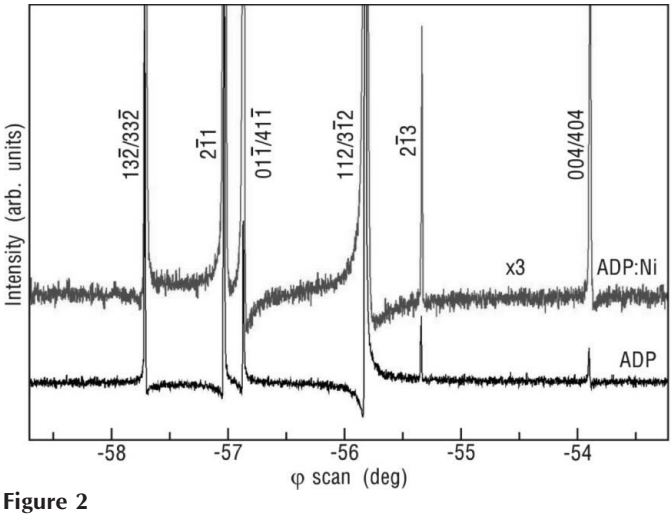

Figure 2
Azimuthal scan of the 400 reflection in ADP and ADP:Ni crystals. M = [001], E = 6480 eV and $\chi = 90°$ (σ polarization). Pairs of indices stand for four-beam cases.

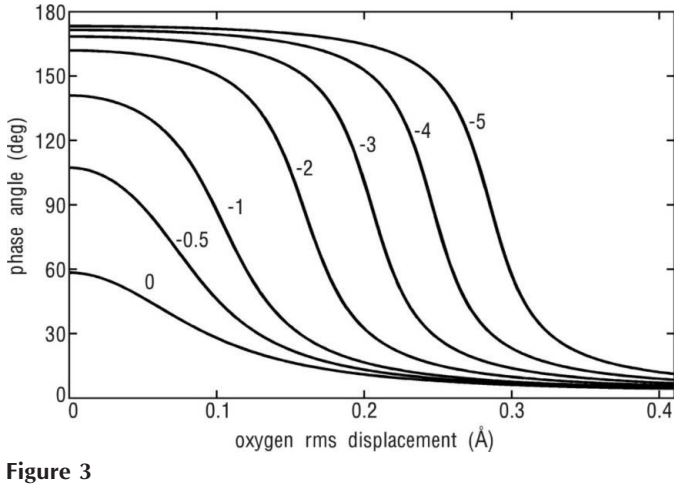

Figure 3
Phase of the 400 reflection as a function of the oxygen r.m.s. displacement in the ADP:Ni sample. Values of the parameter Δ, defined in equation (4), are shown beside each curve.

Table 2
Theoretical triplet phases in KDP, Ψ, and their respective ΔΨ shifts obtained by fitting with $L(\varphi)$ [equation (3)] the experimental data from samples KDP:Mn1 and KDP:Mn5.

Phase values are given in degrees and $\Psi' = \Psi + \Delta\Psi$.

	KDP	KDP:Mn1		KDP:Mn5	
XRMD	Ψ	ΔΨ	Ψ′	ΔΨ	Ψ′
$11\bar{2}$&152	33.6	11 (5)	45 (5)	29 (5)	62 (5)
$15\bar{2}$&112	−24.3	−6 (5)	−30 (5)	−21 (5)	−45 (5)

as a function of the oxygen r.m.s. displacement, $\langle \mathbf{u}^2 \rangle^{1/2}$, for different values of Δ. Contributions of atomic resonances to the scattering amplitudes are responsible for the slopes of the curves. In the absence of resonances, whose strongest contribution is from the P atoms, the curves would be sharper steps providing phase shifts of 180°. The used values of atomic resonances, f' and f'', are given in Appendix *B*. According to the curves in Fig. 3, large phase shifts of more than 100° in δ_A are possible if $\Delta < -1$ and $\langle \mathbf{u}^2 \rangle^{1/2} > 0.3$ Å. This r.m.s. value is of the same order as the expected thermal parameters for this family of materials at room temperature (Fukami & Chen, 2006), but it can shift δ_A because it is affecting only the oxygen contribution in equation (4).

Although the choice of a weak primary reflection can favor the occurrence of large phase shifts, which is helpful in providing enhanced signals relating to possible effects of dopant ions in the crystal lattice, it is inappropriate for quantitative phase analysis because the amplitude of the primary wave is much smaller than the amplitude of the secondary wave. Since the phase information derives from the interference of these waves, they must be waves of comparable strength, *i.e.* with amplitudes of the same order, to allow phase determination with good accuracy.

4.2. KDP

Slight variations in the φ profiles, without inversion of asymmetry, can also be evidence of structural changes. Experimental profiles of the three-beam cases $11\bar{2}$&152 and $15\bar{2}$&112 in the KDP, KDP:Mn1 and KDP:Mn5 samples are compared in Fig. 4. The 260 reflection (reflection *A*) has been chosen because of the low symmetry of the reciprocal space around the [130] direction, which favors the occurrence of individual three-beam cases. To enhance the profile sensitivity for triplet phase analysis, the strength of the 260 reflection was reduced by tuning the X-ray energy to $E = 7440$ eV (Bragg angle of 45°) and the polarization angle from $\chi = 90°$ (σ polarization) to $\chi = 32°$.

As can be clearly seen in Fig. 4, the experimental profiles of the $11\bar{2}$&152 and $15\bar{2}$&112 cases of XRMD vary systematically with the Mn content. The profiles correspond to out–in positions, and such variations indicate triplet phases shifting in the opposite sense: $\Delta\Psi > 0$ ($\Delta\Psi < 0$) for $11\bar{2}$&152 ($15\bar{2}$&112). By using the line-profile function $L(\varphi)$ [equation (3)], the ΔΨ values in each case could be obtained within an error bar of ±5°, as presented in Table 2 (see Appendix *C* for details on the phasing procedure).

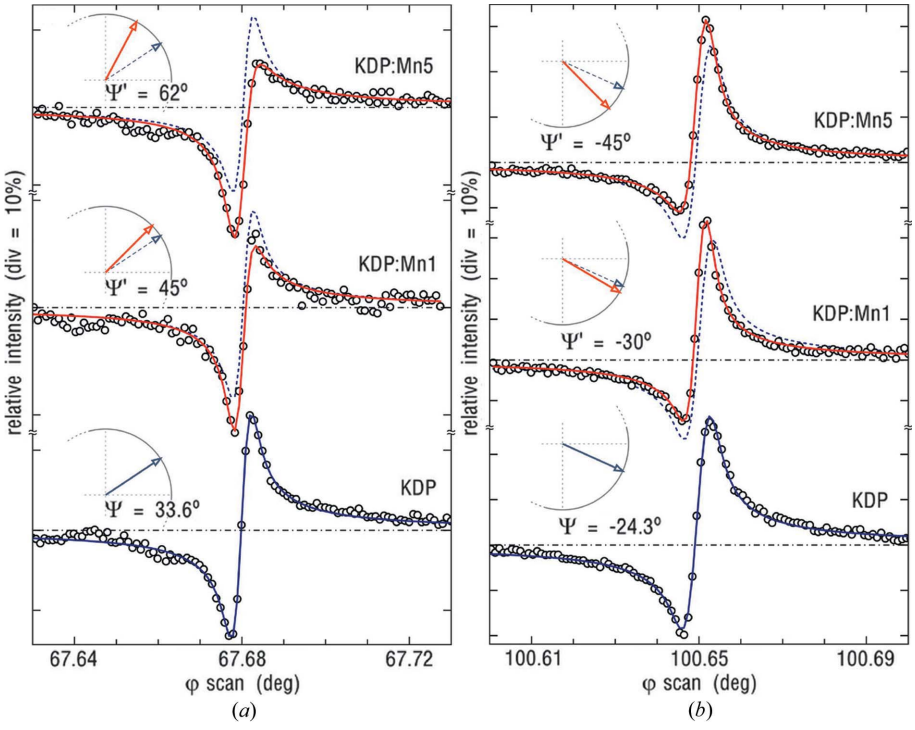

Figure 4
Experimental φ profiles (open circles) in KDP, KDP:Mn1 and KDP:Mn5 samples: (*a*) $11\bar{2}$&152 and (*b*) $15\bar{2}$&112. Triplet phases Ψ′, determined with $L(\varphi)$ fittings (solid lines), are compared with the theoretical Ψ values beside each profile. KDP reference profiles (dashed curves) and horizontal (dashed–dot) lines were used for enhancement of the visual perception of changes in the profiles. M = [001], $E = 7440$ eV and $\chi = 32°$.

To obtain information on structural changes from the measured shifts of triplet phases, model structures are very helpful. In the case of KDP, data on computer modeling of Mn^{2+} ions in the crystal lattice are available. It has been demonstrated that interstitial impurities (dopants) of adequate ionic radius, such as Mn^{2+}, can turn the nearest PO_4 tetrahedron groups by an angle of approximately 6°, favoring the formation of impurity chains and clusters (Rak *et al.*, 2005). We have used a very simple model structure to check if the measured triplet phases can in fact be sensitive to the PO_4 rotation around the *c* axis. The model consists in writing the *x*, *y* and *z* fractional coordinates of the first O atom in the unit cell as a function of the PO_4 rotation angle $\Delta\theta$, so that $x = 0.1698\cos(29.1° + \Delta\theta)$, $y = 0.1698\sin(29.1° + \Delta\theta)$ and $z = 0.1259$. Symmetry operations of the $I\bar{4}2d$ space group provide the coordinates of the other O atoms. $\Delta\theta = 0$

represents the ideal KDP structure. An illustrative view of a structure with rotated tetrahedra, $\Delta\theta \neq 0$, is depicted in Fig. 5.

Using this model, $\Delta\Psi$ shifts were calculated as a function of $\Delta\theta$ for both cases of XRMD, $11\bar{2}$&152 and $15\bar{2}$&112, as shown in Fig. 6. When compared with the experimental data, there is a good agreement of the model with the systematic variation of $\Delta\Psi$ in the series of samples with increasing Mn content (Table 2). This suggests that the average number of rotated PO_4 units increases with the content of Mn^{2+} ions in the crystal lattice and, as a consequence, the average angle of rotation, *i.e.* $\Delta\theta$, also increases. However, before being concerned with more refined model structures, it is important to test the accuracy and reliability of the measured triplet phases.

A test of reliability consists of using the N-beam dynamical theory with Gaussian convolution, $I(\varphi)$, to simulate φ profiles in thin (2 µm) and thick (200 µm) slabs, as well as in both ideal ($\Delta\theta = 0$) and changed ($\Delta\theta = 8.3^\circ$) KDP structures. Then, $L(\varphi)$ fittings are used on simulated data to retrieve the triplet phases and to compare them with the expected (theoretical) values. The simulated φ profiles are shown in Fig. 7. Profile analysis based on the LMAD of function $L(\varphi)$ are shown in Fig. 8, where each XRMD case exhibits distinct responses to this phasing procedure. In the $11\bar{2}$&152 case, the retrieved values of the triplet phases in thick and thin slabs were different (Fig. 8*a*), while in the other case (Fig. 8*b*), the retrieved values were exactly the same.

Reflection B can have either transmission or reflection diffraction geometry. Each geometry may have different effects on how the XRMD profiles vary in response to shifts in the triplet phases. Transmission geometry increases the

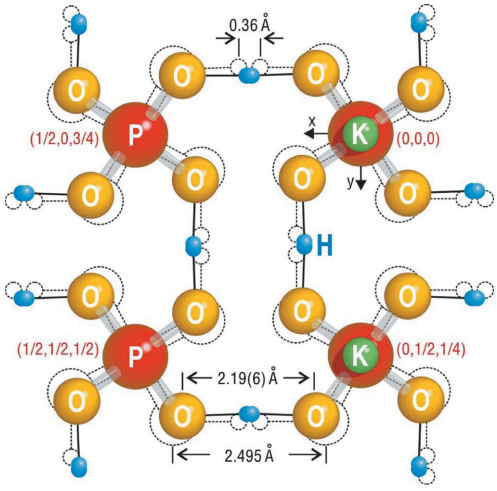

Figure 5
Model structure of KDP with PO_4 units rotated by $\Delta\theta = 8.3^\circ$ with regard to the ideal structure (contours in dashed lines). Atomic radii are not scaled to their actual sizes.

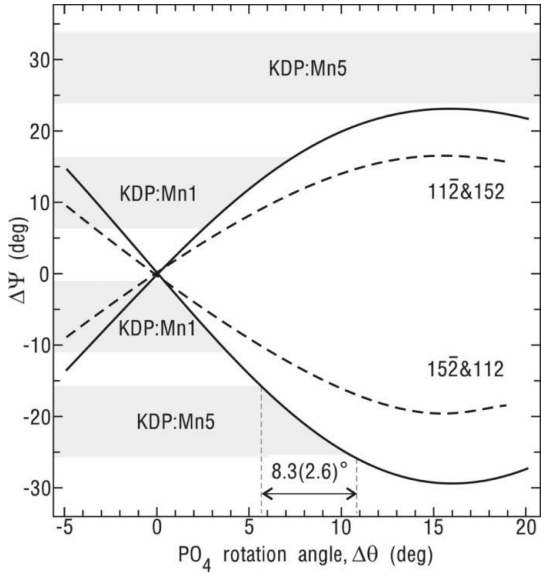

Figure 6
Theoretical $\Delta\Psi$ shifts of triplet phases as a function of the PO_4 rotation angle $\Delta\theta$ for the $11\bar{2}$&152 and $15\bar{2}$&112 cases. Experimental shifts in the KDP:Mn1 and KDP:Mn5 samples (Table 2) are indicated by error bars of $\pm 5^\circ$ (horizontal grey bars). For the sake of comparison, theoretical shifts were calculated assuming either ionized (solid lines) or neutral (dashed lines) atoms (Appendix *B*).

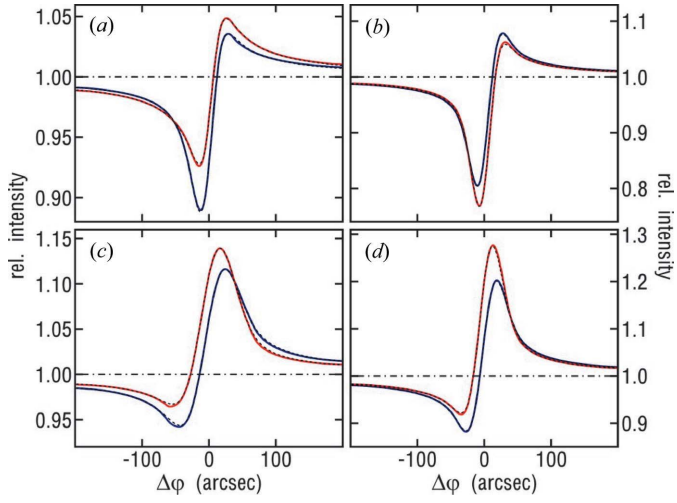

Figure 7
Simulated φ profiles in ideal ($\Delta\theta = 0$, blue curves) and changed ($\Delta\theta = 8.3^\circ$, red curves) KDP structures: (*a*), (*b*) $11\bar{2}$&152 and (*c*), (*d*) $15\bar{2}$&112. Simulation conditions: slab thickness of (*a*), (*c*) 200 µm and (*b*), (*d*) 2 µm, (010) surface, $E = 7440$ eV, and $\chi = 32^\circ$. Best-fitting curves (dashed curves) of $L(\varphi)$ are also shown.

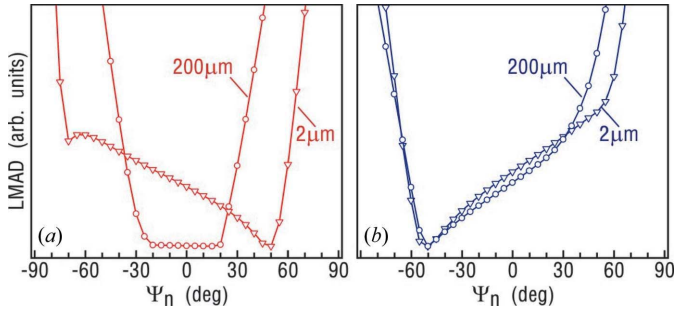

Figure 8
Minimum LMAD values as a function of the trial triplet phases Ψ_n, for the simulated φ profiles in Fig. 7. (*a*) $11\bar{2}$&152 and (*b*) $15\bar{2}$&112 in thin and thick slabs, as indicated.

probability of photon–lattice interactions of third and higher order occurring before the X-ray photons are able to exit the crystal for detection. Therefore, it tends to increase the contribution of high-order terms in the intensity profiles, so that the second-order approach [equation (2)] is no longer valid. $11\overline{2}$&152 is a good example of such a case. Its intensity profiles (Figs. 7*a* and 7*b*) are sensitive to changes in slab thickness, and the shifts of triplet phases are perceived differently in thick and thin slabs. Phase analysis with $L(\varphi)$ (Fig. 8*a*) works better in the thin slab since the second-order approach becomes valid with a reduction of thickness. In the other case, $15\overline{2}$&112, the reflection geometry practically eliminates any contribution of high-order terms. The profile is therefore insensitive to changes in the slab thickness (Figs. 7*c* and 7*d*), and triplet phase retrieval with the second-order approach works very well in both thin and thick slabs, as can be seen in Fig. 8(*b*).

In bulk crystals, the phase coherence of high-order terms can be detuned by lattice imperfections. This implies that phase analysis based on the $L(\varphi)$ function can be, in general, more suitable for samples of poorer crystalline quality, such as doped crystals, than for highly perfect crystals. However, when using reference φ profiles from real crystals, the actual contributions of high-order terms are difficult to quantify. As a consequence, the accuracy in measuring relative triplet phases from reference to doped samples becomes compromised for most cases of XRMD. Exceptions are those cases where the absolute predominance of the second-order term in the perfect-crystal profile can be verified. According to the theoretical test of reliability mentioned above, and with the experimental conditions used in this work [samples with (010) surface, out–in positions, $E = 7440$ eV and $\chi = 32^\circ$], $15\overline{2}$&112 is a reliable case for phasing. It is able to provide accurate phase values with an error bar as small as $\pm 5^\circ$ (Table 2), which can be useful for comparison with model structures of Mn-doped KDP.

Localized changes of the crystal lattice in the vicinity of dopant ions do not seem to be able alone to explain the observed phase shifts. If only local changes are taken into account, the Mn contents obtained from RBS are too small to generate phase shifts with the magnitudes that were observed. Considering the KDP:Mn5 sample, for example, its 0.36 wt% content of Mn is equal to 1/28 dopant ions per unit cell. At interstitial positions like 0.35, 0.25 and 0.125 (Rak *et al.*, 2005; Lai *et al.*, 2005), with eight equivalent sites in the unit cell, the occupation factor of Mn is smaller than 1/200. Even in the case of removing the nearest two K^+ ions to reach the balance of valency, the structure factors will be changed by very small amounts, no larger than $(f_{Mn^{2+}} + 2f_{K^+})/200 < 0.3$, and no measurable phase shifts would result from these changes.

On the other hand, although the PO_4 rotation model appears to be a relatively simple model providing an explanation for the experimental data, it requires a more detailed discussion. The investigated triplet phases are sensitive to PO_4 rotations ranging from 0 to about 16° (Fig. 6). This latter value seems too large to be allowed in the KDP structure without changing any atomic distances other than the length of the O—H—O bridges (Fig. 5). Moreover, to obtain an average rotation angle of $\Delta\theta = 8.3\,(26)^\circ$, almost all PO_4 units, or at least half of them, would have to be rotated in the KDP:Mn5 sample to give rise to the measured phase shift of $\Delta\Psi = 21\,(5)^\circ$. Many other model structures can be proposed, and perhaps some of them could provide different explanations for the observed variations in φ profiles as a function of the Mn content in the samples. Otherwise, the experimental data suggest a mechanism of internal stress in KDP, where a single Mn^{2+} ion is rotating not only the nearest PO_4 groups, as predicted by computer modeling (Rak *et al.*, 2005), but many groups within at least two tens of unit cells.

5. Conclusions

This work has demonstrated that reflection phases are sensitive to the presence of dopant ions in the lattice of NLO crystals. It offers a new tool for studying doping effects in this kind of material. Two strategies for phase measurements by multiple diffraction experiments were also demonstrated: (i) weak primary reflection susceptible to large phase shifts providing a clear signal of the effects of doping; and (ii) XRMD with diffracted waves of comparable strength properly adjusted for accurate phasing with an error bar of $\pm 5^\circ$. In the latter, three-beam dynamical simulation is necessary for identifying reliable cases where the phase information can be extracted even in the presence of lattice imperfection (mosaicity). There is, however, a minimum grain size requirement necessary for dynamical coupling of diffracted beams, otherwise no phase information will be available from the interference profiles of the XRMD phenomenon. In the investigated samples, the effects of doping were correlated with the dopant ions occupying interstitial sites close to O—H—O bridges. In ADP:Ni, such interstitial occupation is the probable cause of the increased disorder of oxygen sites that explains the observed shift in the phase of the 400 reflection. In KDP:Mn, the effect of doping seems to be more systematic, driving extended regions of the material into an internally stressed configuration with shortened hydrogen bridges.

APPENDIX *A*
Polarization vectors

The polarization vectors $\mathbf{v}_1 = \hat{\mathbf{k}}_A \times (\hat{\mathbf{v}}_0 \times \hat{\mathbf{k}}_A)$ and $\mathbf{v}_2 = \hat{\mathbf{k}}_A \times \{[\hat{\mathbf{k}}_B \times (\hat{\mathbf{v}}_0 \times \hat{\mathbf{k}}_B)] \times \hat{\mathbf{k}}_A\}$ are computed for each polarization direction $\hat{\mathbf{v}}_0$ of the incident synchrotron radiation (Stetsko *et al.*, 2004). In a given reference system where $\hat{\mathbf{k}}_0 = (0, 0, 1)$ is taken as the incident beam direction and θ_Q as the Bragg angle of reflection Q (= A, B and C), the diffracted beam directions are $\hat{\mathbf{k}}_A = (\sin 2\theta_A, 0, \cos 2\theta_A)$, from reflection A, and $\hat{\mathbf{k}}_B = [x, \pm(\sin^2 2\theta_B - x^2)^{1/2}, \cos 2\theta_B]$, from reflection B. $x = (\cos 2\theta_C - \cos 2\theta_A \cos 2\theta_B)/\sin 2\theta_A$ and the '±' signs correspond to that used in w_S [equation (3)]: '+' ('−') for out–in (in–out) positions. In this system of reference, $\hat{\mathbf{v}}_0 = (-\cos\chi, \sin\chi, 0)$. For $\chi = 0$ the incidence plane of the primary reflection, *i.e.* the plane that contains both $\hat{\mathbf{k}}_0$ and $\hat{\mathbf{k}}_A$

Table 3
Theoretical anomalous scattering coefficients, f' and f'' (Prince, 2004).

	$E = 6480$ eV						$E = 10\,200$ eV	
	N	O	P	K	Mn	Ni	Ga	As
f'	0.0454	0.0707	0.3570	–	–	−1.3226	−3.6749	−1.6580
f''	0.0286	0.0508	0.6514	–	–	0.7543	0.5062	0.6569

	$E = 7440$ eV						$E = 10\,500$ eV	
	N	O	P	K	Mn	Ni	Ga	As
f'	–	0.0565	0.3202	0.3769	−1.0886	–	−3.7146	−1.8269
f''	–	0.0381	0.5039	1.2250	3.1292	–	3.7906	0.6233

versors, is in a horizontal position, corresponding to the π state of linear polarization. At $\chi = 90^\circ$ the incidence plane is vertical, hence in the σ polarization. The minus signal in $\hat{\mathbf{v}}_0$ is a convention owing to the rotation sense of the diffractometer's χ axis (Morelhão, 2003*b*).

APPENDIX *B*
Atomic scattering and structure factors

In calculating the atomic scattering factors $f = f_{\rm Th} + f' + if''$, the Thomson scattering was estimated by using the Cromer–Mann coefficients (Prince, 2004), while the used atomic resonance correction terms, f' and f'', are given in Table 3.

The following crystals were used:

(1) GaAs crystal, cubic lattice: a = 5.6534 Å, space group $F\bar{4}3m$. In calculating the triplet phases presented in Fig. 1, the origin (0, 0, 0) was set at As with Ga at (0.25, 0.25, 0.25).

(2) ADP crystal, tetragonal lattice: $a = b = 7.4997$, $c = 7.5494$ Å, space group $I\bar{4}2d$. Origin set at P with the first O atom at (0.1466, 0.0843, 0.1151), which leads to $F_{\rm ADP}(h00) \simeq 4[f_{\rm P} + f_{\rm N} + 2(\cos 2\pi hx + \cos 2\pi hy)f_{\rm O}]$ as the structure factor for $h00$ reflections.

(3) KDP crystal, tetragonal lattice: $a = b = 7.4521$, $c = 6.9740$ Å, space group $I\bar{4}2d$. Origin set at P with the first O atom at (0.1484, 0.0826, 0.1259). The effective charges of the K^+, P^{5+} and O^{2-} ions (+0.98e, +1.80e and −1.14e, respectively; Rak *et al.*, 2005) were taken into account in the atomic scattering factors as follows: $f_{K^+} = f_K - 0.98$; $f_{P^{5+}} = f_P - 1.80$; and $f_{O^{2-}} = f_O + 1.14$. Examples of structure factor values required for N-beam dynamical simulations are given in Table 4

APPENDIX *C*
Phasing procedure

For a chosen XRMD case, the $\Delta\Psi$ shift of the triplet phase was determined with respect to a reference φ profile of known triplet phase Ψ. With both profiles in hand, one as the reference and the other from the doped structure, the $L(\varphi)$ fitting procedure was carried out in two steps:

(1) A pair of values for R and g, *e.g.* R_0 and g_0, was obtained by fitting the reference profile with the known value of Ψ, and with no boundaries imposed for the parameter–vector **p**

Table 4
Structure factors, modulus $|F|$ and phase δ of the $hk\ell$ reflections required for N-beam dynamical simulation of $15\bar{2}$&112 XRMD in ideal ($\Delta\theta$ = 0) and changed ($\Delta\theta = 8.3^\circ$) KDP structures.

$E = 7440$ eV, $\Delta\theta = 0$.

$hk\ell$	000	260	$\bar{2}60$	$15\bar{2}$	$\bar{1}5\bar{2}$	112	$\bar{1}\bar{1}2$
$\lvert F\rvert$	274.9	78.0	78.0	61.4	62.0	101.7	107.4
δ (°)	1.57	5.24	5.24	3.86	9.00	−22.92	29.84

$E = 7440$ eV, $\Delta\theta = 8.3^\circ$.

$hk\ell$	000	260	$\bar{2}60$	$15\bar{2}$	$\bar{1}5\bar{2}$	112	$\bar{1}\bar{1}2$
$\lvert F\rvert$	274.9	62.3	62.3	63.4	67.7	104.3	110.6
δ (°)	1.57	6.43	6.43	−13.66	25.19	−26.14	32.70

except that ξ and g are constrained in the interval [0, 1] so as to have physical meaning in equation (3).

(2) The obtained R_0 and g_0 pair was used as input for fitting the profile from the doped structure/sample with a trial triplet phase Ψ_n, taken from a set of possible values. For out–in (in–out) positions and destructive/constructive (constructive/destructive) asymmetries $\Psi_n \in [-90, 90^\circ]$, otherwise $\Psi_n \in [90, 270^\circ]$.

During step 2, tight boundaries were used only on parameters R and g, otherwise the inaccuracy in the triplet phase values can be as large as $\pm 90^\circ$ (Morelhão *et al.*, 2005*b*). We have used $\Delta R/R = \pm 0.1$ and $\Delta g/g = 0$, *i.e.* $0.9R_0 < R < 1.1R_0$ and $g = g_0$, when phasing both the experimental and the dynamical simulated profiles. A plot of the minimum LMAD value [minimized with a genetic algorithm (Wormington *et al.*, 1999)] as a function of Ψ_n leads to $\Delta\Psi$, as well as to its respective accuracy.

This work has been supported by FAPESP, CNPq and LNLS.

References

Authier, A. (2005). *Dynamical Theory of X-ray Diffraction*, revised ed. Oxford University Press.
Avanci, L. H., Cardoso, L. P., Girdwood, S. E., Pugh, D., Sherwood, J. N. & Roberts, K. J. (1998). *Phys. Rev. Lett.* **81**, 005426.
Chang, S.-L. (1984). *Multiple Diffraction of X-rays in Crystals.* Berlin, Heidelberg, New York: Springer Verlag.
Chapman, L. D., Yoder, D. R. & Colella, R. (1981). *Phys. Rev. Lett.* **46**, 1578–1581.
Colella, R. (1974). *Acta Cryst.* A**30**, 413–423.
Fukami, T. & Chen, R.-H. (2006). *J. Phys. Soc. Jpn*, **75**, 074602.
Giacovazzo, C. (2002). *Fundamentals of Crystallography*, 2nd ed. Oxford, New York: Oxford University Press.
Hart, M. & Lang, A. R. (1961). *Phys. Rev. Lett.* **7**, 120–121.
Juretschke, H. J. (1982). *Phys. Rev. Lett.* **48**, 1487–1489.
Lai, X., Roberts, K. J., Bedzyk, M. J., Lyman, P. F., Cardoso, L. P. & Sasaki, J. M. (2005). *Chem. Mater.* **17**, 4053–4061.
Lipscomb, W. N. (1949). *Acta Cryst.* **2**, 193–194.
Morelhão, S. L. (2003*a*). *Acta Cryst.* A**59**, 470–480.
Morelhão, S. L. (2003*b*). *J. Synchrotron Rad.* **10**, 236–241.
Morelhão, S. L., Avanci, L. & Kycia, S. (2005*a*). *Nucl. Instrum. Methods Phys. Res. Sect. B*, **239**, 245–249.
Morelhão, S. L., Avanci, L. & Kycia, S. (2005*b*). *Nucl. Instrum. Methods Phys. Res. Sect. B*, **238**, 180–184.
Morelhão, S. L. & Kycia, S. (2002). *Phys. Rev. Lett.* **89**, 015501.

Post, B. (1977). *Phys. Rev. Lett.* **39**, 760–763.
Prince, E. (2004). Editor. *International Tables for Crystallography*, Vol. C, 3rd ed. Dordrecht: Kluwer Academic Publishers.
Rak, M., Eremin, N. N., Eremina, T. A., Kuznetsov, V. A., Okhrimenko, T. M., Furmanova, N. G. & Efremova, E. P. (2005). *J. Cryst. Growth*, **273**, 577–585.
Reeuwijk, S. J. V., Puig-Molina, A. & Graafsma, H. (2000). *Phys. Rev. B*, **62**, 6192–6196.
Remédios, C. M. R., Paraguassu, W., Freire, P. T., Mendes-Filho, J., Sasaki, J. M. & Melo, F. E. (2005). *Phys. Rev. B*, **72**, 014121.
Renninger, M. (1937). *Z. Kristallogr.* **97**, 107–121.
Rossmanith, E. (1992). *Acta Cryst.* A**48**, 596–610.
Rossmanith, E. (2007). *Acta Cryst.* A**63**, 251–256.
Santos, A. O. dos, Lang, R., Menezes de, A. S., Meneses, E. A., Reboh, L. A. S. & Cardoso, L. P. (2009). *J. Phys. D Appl. Phys.* **42**, 195401.
Shen, Q. (1998). *Phys. Rev. Lett.* **80**, 3268–3271.
Shen, Q. & Colella, R. (1987). *Nature* (*London*), **329**, 232–233.
Shen, Q., Elfimov, I. S., Fanwick, P., Tokura, Y., Kimura, T., Finkelstein, K., Colella, R. & Sawatzky, G. A. (2006). *Phys. Rev. Lett.* **96**, 246405.
Shen, Q., Kycia, S. & Dobrianov, I. (2000). *Acta Cryst.* A**56**, 264–267.
Stetsko, Y. P., Juretschke, H. J., Huang, Y.-S., Chao, C.-H., Chen, C.-K. & Chang, S.-L. (2000). *Acta Cryst.* A**56**, 394–400.
Stetsko, Yu. P., Juretschke, H. J., Huang, Y.-S., Lee, Y.-R., Lin, T.-C. & Chang, S.-L. (2001). *Acta Cryst.* A**57**, 359–367.
Stetsko, Y. P., Lee, Y.-R., Tang, M.-T. & Chang, S.-L. (2004). *Acta Cryst.* A**60**, 64–74.
Thorkildsen, G., Larsen, H. B., Weckert, E. & Semmingsen, D. (2003). *J. Appl. Cryst.* **36**, 1324–1333.
Tischler, J. Z. & Batterman, B. W. (1986). *Acta Cryst.* A**42**, 510–514.
Weckert, E. & Hümmer, K. (1997). *Acta Cryst.* A**53**, 108–143.
Wormington, M., Panaccione, C., Matney, K. M. & Bowen, D. K. (1999). *Philos. Trans. R. Soc. London Ser. A*, **357**, 2827–2848.